Article

Evolution of Photoluminescent CdS Magic-Size Clusters Assisted by Adding Small Molecules with Carboxylic Group

Zhengtian He, Dongqing Wang, Qiyu Yu, Meng Zhang, Shanling Wang, Wen Huang, Chaoran Luan,* and Kui Yu*

Read Online

ACCESS | Metrics & More | Article Recommendations | SI Supporting Information

ABSTRACT: We report our investigation on the formation of photoluminescent CdS magic-size clusters (MSCs), which exhibit absorption peaking at 373 nm, along with sharp band edge emission at ~385 nm. Denoted as MSC-373, the MSCs were synthesized from the reaction of cadmium oleate ($Cd(OA)_2$) and S powder in 1-octadecene at room temperature, together with the addition of acetic acid (HOAc) or acetate salts ($M(OAc)_2$, M = Zn and Mn) during the prenucleation stage (120 °C). The morphology of as-synthesized MSC-373 was dot-like, which could be altered to flake-like morphology after purification. We found the formation of MSC-373 was related to the ligand exchange, resulting from the addition of small molecules with carboxylic group. The addition of HOAc not only promotes the formation of CdS MSC-373 but suppresses the formation of MSC-311 and nucleation and growth of quantum dots (QDs). When the amount of HOAc addition was increased, another photoluminescent CdS MSCs, namely, MSC-406, evolved. This study provides an overall understanding of the CdS MSC-373 and introduces a new approach to synthesize photoluminescent CdS MSCs.
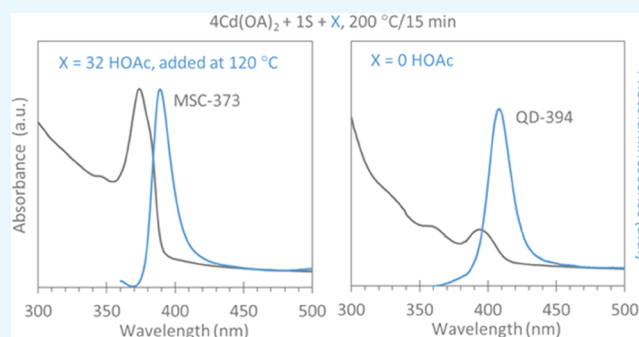
1. INTRODUCTION

Colloidal photoluminescent semiconductor quantum dots (QDs) have received much attention over the past decades for their size-dependent electronic transitions, which may be potentially used in fields as imaging, biomedical, and security technology.[1−8] However, less attention has been paid to the formation of photoluminescent magic-size clusters (MSCs), which consist of a discrete number of atoms with the size of 1–3 nm.[9−17] Known as co-products in the production of colloidal QDs, MSCs display different properties from QDs in many aspects.[18−21] For example, compared to QDs, MSCs usually exhibit narrower optical bandwidths due to tighter size distributions. Also, for samples extracted in sequence from a reaction batch, the MSCs usually show optical absorption peaks at fixed wavelengths, while the QDs exhibit optical absorption peaks featured with redshift as their size increases.

Recently, a two-pathway model has been proposed for the formation of QDs as well as MSCs.[22−24] This model suggested that there are two individual but linked pathways during the prenucleation stage of colloidal metal (M = Cd and Zn) chalcogenide (E = S, Se, and Te) QDs. For one pathway, monomers and fragments formed via the covalently bonding between M−E precursors in the prenucleation stage. Subsequently, nucleation and growth of QDs took place, as suggested by the conventional LaMer model of the classical nucleation theory (CNT).[25−28] For the other pathway, the self-assembly of M and E precursors occurred first, followed by the formation of M−E covalent bonds within the assembled aggregates at a relatively high temperature. The bonding species, precursor compounds (PCs), which are transparent in optical absorption, would transform to MSCs via the intramolecular organization.[22−24,29−31] The formation pathways of QDs and MSCs were connected by PCs, via a transformation from MSCs to PCs, followed by the fragmentation of PCs to support the nucleation and growth of QDs.

Based on the two-pathway model, a two-step approach was further proposed to produce MSCs, to avoid the contamination of QDs. The first step is the preparation of the PCs at a relatively high reaction temperature in the prenucleation stage. The second step is the transformation of PC-to-MSC at a relatively low reaction temperature. With the two-step approach, a series of MSCs were obtained without QDs, such as CdS MSC-311, CdSe MSC-415, CdTe MSC-371, and ZnSe MSC-269.[22,29−35] Moreover, a modified one-step
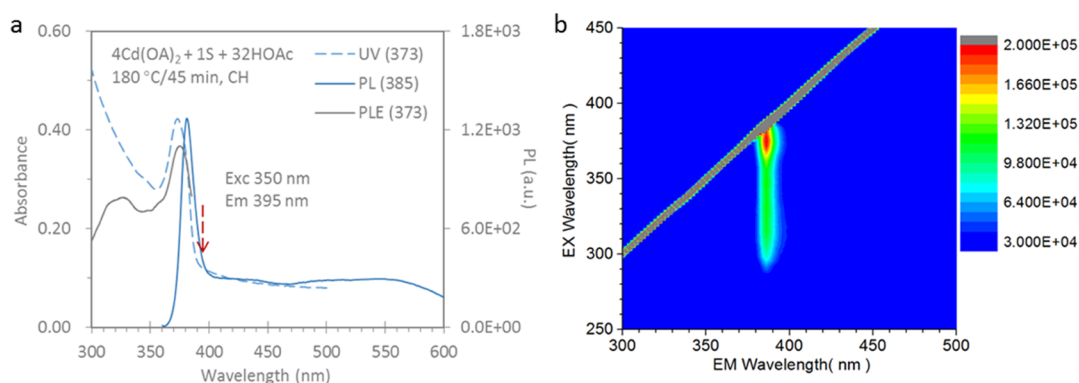
Figure 1. (a) Normalized PLE (gray trace, with the corresponding emission wavelength indicated by dashed red arrow, right *y* axis), optical absorption (dashed blue trace, left *y* axis), and emission (solid blue trace excited at 350 nm, right *y* axis) spectra and (b) 3D PL contour mapping of CdS MSC-373. With the feed molar ratio of 4Cd-1S-32HOAc, the addition of HOAc was performed under a N_2 atmosphere at 120 °C. The sample was extracted when the temperature was held at 180 °C for 45 min. A volume of 25 μL of the extracted sample was dispersed in 3.0 mL of cyclohexane (CH) for the optical study. Obviously, a photoluminescent CdS MSCs was obtained, which exhibits absorption peaking at 373 nm and emission peaking at 385 nm, thus denoted by MSC-373. It was noteworthy that CdS MSC-373 was obtained without the coproduction of QDs. The excitation wavelength range was from 290 to 380 nm.

approach was presented to achieve MSCs directly at high temperatures, without the generation of QDs.[24,36−39] The key of the one-step approach is the small molecular acid additive, such as acetic acid (HOAc), which was added in the reaction with M and E precursors. For CdSe MSCs, photoluminescent CdSe dMSC-460 evolved with the addition of HOAc, which exhibits optical absorption doublet peaking at 433/460 nm and PL at 463 nm. The small molecule addition suppresses the nucleation and growth of QDs and promotes the formation of MSCs.[37] Moreover, it was found that the self-assembly of zero-dimension (0D) NCs into two-dimension (2D) wells can be induced by the use of ethanol (EtOH) during purification.[38] Also, CdTe dMSC-427 (with optical absorption doublet peaking at 385/427 nm and PL at 429 nm) was produced with HOAc additive. It was demonstrated that the solubility of the Cd precursor, such as $Cd(OA)_1(OAc)_1$, was critical to the production of MSCs or QDs.[36] CdS MSCs were reported to synthesize with photoluminescent property,[17,40,41] while the small molecule addition assisted one-step approach has not been explored.

Here, we report the synthesis of photoluminescent CdS MSC-373 without the co-production of QDs. The formation of MSC-373 was from the reaction of $4Cd(OA)_2$ + 1S in 1-octadecene (ODE) at room temperature, with a S concentration of 30 mmol/kg, when HOAc or $M(OAc)_2$ (M = Zn and Mn) was added in the prenucleation stage at 120 °C. Figure 1 demonstrates the optical property of the photoluminescent CdS MSC-373. Figure 2 shows the morphological change of MSC-373 before and after the purification process by transmission electron microscopy (TEM). Figure 3 studies the formation of MSC-373 with different carbon-chain length of the acids. Figure 4 explores the effect of the HOAc addition on the formation MSC-373. Figure 5 presents the evolution of another photoluminescent CdS MSC-406 with a larger amount of HOAc addition. The current study elucidates the effect of small molecule additives with carboxylic group in the evolution of photoluminescent CdS MSCs, which may contribute to more understanding of the nanocrystal synthesis on the molecular level.

2. RESULTS AND DISCUSSION

2.1. Optical Properties of CdS MSC-373. Figure 1 shows the optical properties of the CdS MSCs prepared with the addition of HOAc. For the reaction, 0.60 mmol of $Cd(OA)_2$ and 0.15 mmol of S powder were mixed in ODE at room temperature, with a S concentration of 30 mmol/kg. The addition of 4.80 mmol of HOAc was performed under a N_2 atmosphere at 120 °C after evacuation. Then, the reaction temperature was increased and kept at 180 °C, sampling occurred at (1) 5 min, (2) 10 min, (3) 15 min, (4) 30 min, (5) 45 min, (6) 60 min, (7) 90 min, (8) 120 min, and (9) 180 min, as shown by Figure S1. The sample (25 μL) extracted at 180 °C/45 min was dispersed in 3.0 mL of cyclohexane (CH) for the spectroscopy study.

As shown in Figure 1a, in absorption spectrum (dashed blue trace), a sharp peak was observed at ~373 nm with a red-side shoulder at ~382 nm, which indicates the formation of a type of CdS MSCs, denoted as MSC-373. The PL spectrum (solid blue trace) of MSC-373 displays an extremely sharp band gap emission peaking at ~385 nm with the full width at half maximum (FWHM) as small as 12 nm. Moreover, it was found that the reliable excitation wavelength was from around 290 to 380 nm (Figure 1b). When the emission wavelength is set at 395 nm, the PLE spectrum (solid gray trace) presents the lowest-energy peak at 373 nm and another broad peak at 320 nm. In Figure S1a, CdS MSC-373 and MSC-328 were obtained at 180 °C /5 min, and the amount of MSC-373 increased with MSC-328 decreased gradually during the reaction period from 5 to 15 min. Afterward, only MSC-373 was observed after 30 min. Figure S1b indicates the evolution of optical absorption properties of MSC-373. With the background absorbance wavelength at 388 nm, the optical density (OD) value of MSC-373 monotonously increased from 0.05 (5 min) to 0.30 (60 min) and then decreased to 0.25 (180 min). Figure S2 presents the additional PLE spectra of MSC-373 with different excitation wavelengths. When the emission is set on the blue side or at the center of the PL peak (Figures S2a and S2b), the PLE spectra show two small peaks at 353 and 327 nm. When the emission is set on the red side of the PL peak (Figure S2c,d), the PLE spectrum shows two peaks at 373 and 390 nm in Figure S2c or one peak at 373 nm in Figure S2d. Figure S3 presents the evolution of optical properties of
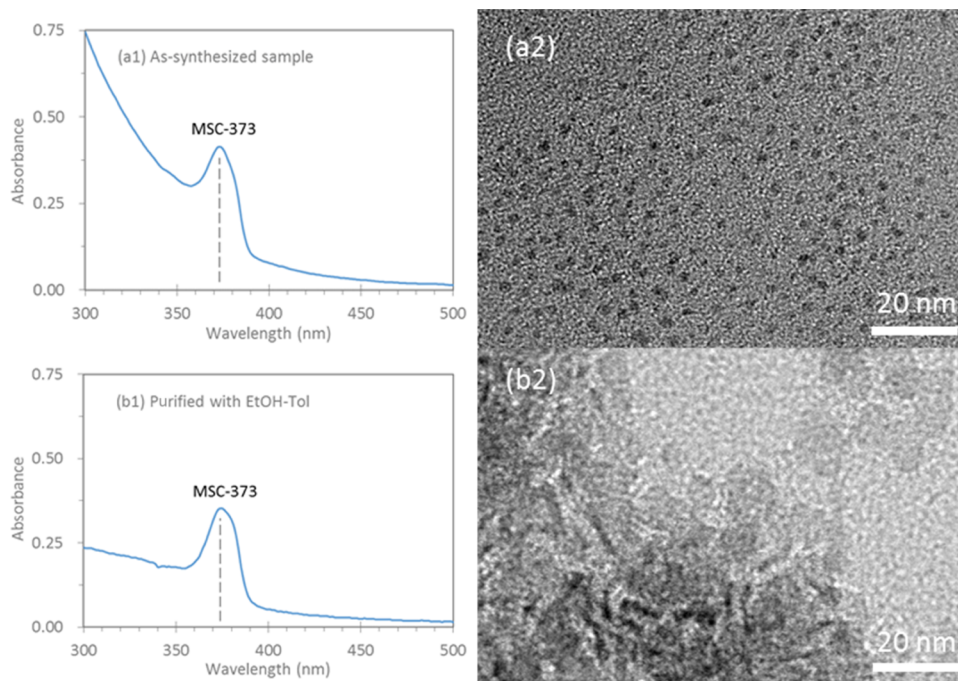
Figure 2. Optical absorption spectra (left panel) and corresponding TEM images (right panel) obtained from the samples of MSC-373 before (a) and after (b) purification. For a1 and a2, 25 μL of the as-synthesized CdS sample was dispersed in 3.0 mL of CH for the spectroscopy and TEM study; For b1 and b2, the CdS sample was purified with the mixture of Tol (2.0 mL) and EtOH (1.0 mL) and then dispersed in 3.0 mL of CH for the spectroscopy and TEM study. Evidently, the morphology of as-synthesized MSC-373 was dot-like, which was changed to be flake-like after the purification.

CdS samples with the reaction temperature from 140 to 240 °C. The samples were extracted from the reaction batch similar to the batch in Figure S1. The optical measurement was performed immediately (top panel) and after 1 day incubation (bottom panel). The formation of CdS MSC-373 started at 180 °C (trace 3), and the amount of MSC-373 increased when the temperature was heated to 240 °C (trace 6). It was noteworthy that the absorption and emission spectra of MSC-373 changed little after 1 day incubation. Figures S3a2 and S3b2 show broad trap emission at ∼540 nm when the temperature increased to 220 °C (trace 5) and 240 °C (trace 6). Figure S4 displays the absorption spectra of two different dispersion of CdS MSC-373. It was found that both CH and toluene (Tol) are suitable for the optical measurement of CdS MSC-373. The difference in density of MSC-373 in dispersions is due to the different extinction coefficients of the dispersions.

CdS MSC-373 with extremely sharp band edge PL peaking at 385 nm was obtained without the coexistence of QDs, when 32 equivalent of HOAc was added in the prenucleation stage. When the emission wavelength was fixed on the red side of the PL peak, the PLE spectra showed the lowest-energy peak at 373 nm, which implies that MSC-373 was the single luminescent source. CdS MSC-373 still existed even at a relatively high reaction temperature (240 °C) and changed little after 1 day incubation, which suggests that MSC-373 was stable. In a side note, another type of CdS MSCs exhibiting one broad absorption peaking at 328 nm was observed at a relatively low reaction temperature (160 °C) with the assistance of HOAc, as shown in Figure S3a1.

2.2. Characterization. To advance our understanding of CdS MSC-373, conventional characterization tools including TEM, Fourier transform infrared absorption spectroscopy (FTIR), energy-dispersive spectrometry (EDS), X-ray photo-

electron spectroscopy (XPS), and powder X-ray diffraction (XRD) were carried out. Figure 2 presents the absorption spectra (left panel) and corresponding TEM images (right panel) of CdS MSC-373 samples before (top panel) and after purification (bottom panel). The sample was extracted from the reaction batch similar to the batch in Figure 1 but held at 200 °C for 15 min. The same absorption peak at ∼373 nm was detected in both samples. Moreover, a noticeable decrease in the absorbance at the shorter wavelengths (300−350 nm) was observed in Figure 2b1, compared to the absorption of the as-synthesized sample (Figure 2a1). It was reported that the absorption at the shorter wavelengths was associated with the monomers and fragments, which formed at the prenucleation stage.[42] Thus, it seems that the purification process effectively removed the monomers and fragments while kept the absorption property of MSC-373.

Interestingly, the TEM images displayed that the morphology of as-synthesized CdS MSC-373 was mainly dot-like with an average size of ∼2 nm; after the purification, the flake-like structure was observed. Figure S5 presents the TEM images with the scale bar of 50 nm. Regarding what we mentioned above, it was found out that the underlying cause for morphologic change was likely due to the purification solvent of EtOH.[38,43] The protic agent of EtOH might increase the surface energy via striping the carboxylate ligand from CdS MSC-373 (details discussed in Figure S6 with the FTIR study), leading to the 0D structure to form the 2D structure via self-assembly. It should be pointed out that, for the as-synthesized MSCs without purification, the organic matters are invisible in the TEM images, which was also reported in CdSe MSC-463.[38]

In order to study the chemical composition of MSC-373, EDS measurement was carried out. Table S1 illustrates the
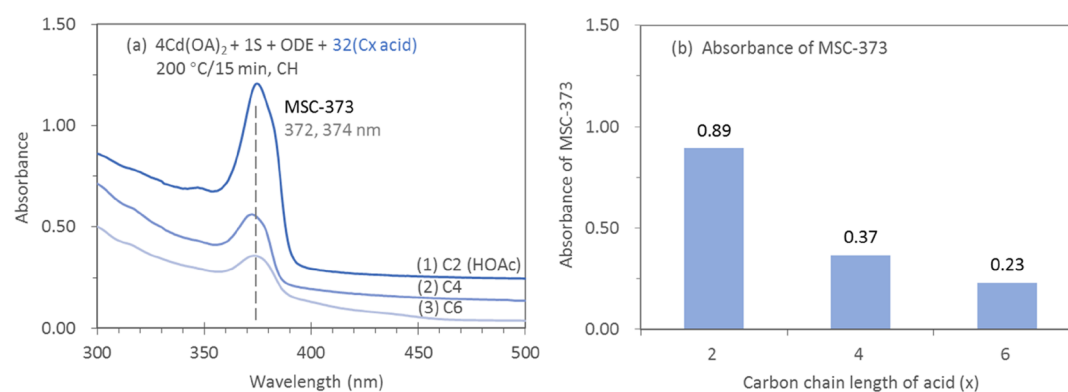
Figure 3. Optical absorption spectra (a) (offset) of three as-synthesized CdS samples (200 °C/15 min) extracted from batches with the addition of three different carbon-chain length of the acids and its corresponding absorbance (b) of the resulting MSC-373 (at the lowest energy peak subtracted by OD$_{400}$). With the feed molar ratio of 4Cd to 1S to 32 acid, the addition of the acids was performed at 120 °C under a N$_2$ atmosphere after an evacuation for 30 min. The reaction temperature was increased from 140 to 240 °C in steps of 20 °C, and six samples were taken after a 15 min of holding time at each temperature. For the optical spectroscopy study, an aliquot (25 μL) of each as-synthesized sample was dispersed in 3.0 mL of CH. Obviously, the amount of MSC-373 evolved at 200 °C/15 min decreased with the increase in the carbon-chain length.

EDS analysis at three different areas of the purified CdS MSC-373 sample, and the reaction batch and purification method were similar to the batch in Figure 2. With the results of each elemental composition for the three areas, the ratios of Cd to S and C to O are summarized in Table S1. The mean atom ratio of Cd to S was about 2:1, and C to O was about 5:1. For the former, the XPS analysis (Figure S7) proposed that the ratio of Cd to S was about 1.85, which is in agreement with the EDS results that MSC-373 has a Cd-rich composition. The results support that the synthetic strategy of a high Cd to S feed molar ratio benefits the formation of MSC-373. For the latter, it implies that the initial ligand of HOA (C to O atom ratio of 9:1) had been replaced partially by HOAc (C to O atom ratio of 1:1), which is in agreement with the FTIR results in Figure S6. The partial ligand exchange on the Cd atom was also proposed in the formation of CdTe dMSC-427, in which the signals of two types of ligands were observed with ^{13}C NMR.[36] The ligand exchange after the addition of HOAc was reported in the evolution of CdTe dMSC-427, where an equilibrium equation (eq 1) has been proposed.[36]

$$Cd(OA)_2 + HOAc \Leftrightarrow Cd(OA)_1(OAc)_1 + HOA \quad (1)$$

Here, we also proposed that the ligand exchange occurred, which resulted in the formation of CdS MSC-373. To explore the structure of MSC-373, XRD measurement of the purified MSC-373 sample was performed. As indicated by Figure S8, the diffraction pattern was similar to the cubic structure of CdS bulk, with three noticeable diffraction peaks of (111), (220), and (311). Table S2 shows the size calculation of purified MSC-373, which is about 1.94 nm.

2.3. Study on the Formation of MSC-373. Figure 3a demonstrates the absorption spectra extracted at 200 °C/15 min from three batches with different carbon-chain length of the acids. Similar to that in Figure 1, the addition of 4.80 mmol of acetic acid (C2 acid, HOAc, batch 1), butyric acid (C4 acid, batch 2), and hexanoic acid (C6 acid, batch 3) was performed at 120 °C. Figure 3b summarizes the OD value of CdS MSC-373 of three samples, deducted the background absorbance at 400 nm. With the increase in carbon-chain length, the amount of MSC-373 produced at 200 °C/15 min decreased from 0.89 (trace 1) to 0.23 (trace 3). Figure S9 shows the whole evolution of optical absorption properties of the samples from batches 1 to 3; a stepwise heating was carried out from 140 to

240 °C in steps of 20 °C, and sampling occurred after holding for 15 min at each temperature. With C2 acid (Figure S9a), MSC-328 was observed temporarily at 160 °C (trace 2) and 180 °C (trace 3), and completely gone at 200 °C (trace 4). MSC-373 appeared at 180 °C (trace 3) and developed till 240 °C (trace 6). With C4 acid (Figure S9b), MSC-328 was only observed at 180 °C (trace 3). MSC-373 was observed during the temperature from 180 to 240 °C (traces 3−6). With C6 acid (Figure S9c), MSC-322 was observed at 180 °C (trace 3), but it no longer existed with the temperature increasing. The signature of MSC-373 appeared at 180 °C (trace 3); afterward, MSC-373 developed and disappeared eventually at 240 °C (trace 6).

It seems that the carbon-chain length of the acids plays an important role in the evolution of MSC-373. The amount of MSC-373 decreased with the chain length increasing. This trend is likely to be related to the extended exchange reaction reported in the acid-assisted evolution of CdTe MSCs (eq 2).[36]

$$Cd(OA)_2 + CH_3(CH_2)_nCOOH$$
$$\Leftrightarrow Cd(OA)_1(CH_3(CH_2)_n COO)_1 + HOA \quad (2)$$
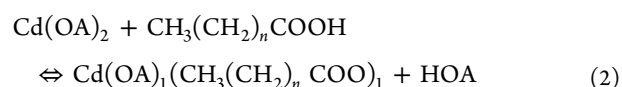
When the length of the carbon-chain increases, the pK_a value of acids increases,[44,45] which suggests the acidity and dissociation capability decrease, resulting in a left shift of the equilibrium (eq 2) and the decline of Cd-$(OA)_1(CH_3(CH_2)_nCOO)_1$ production. In the present study, it is easy to understand that the longer the length, the better solubility of $Cd(OA)_1(CH_3(CH_2)_nCOO)_1$ in ODE, which results in the PC of MSC-373. To support our hypothesis that the ligand exchange caused MSC-373 formation, acetate salts were used as additives in the reaction. As shown in Figure S10, MSC-373 was produced in both samples with acetate addition. Obviously, with Zn(OAc)$_2$ addition (Figure S10a), a relatively larger amount of MSC-373 was observed, compared to that with Mn(OAc)$_2$ addition (Figure S10b). In a side note, a tiny peak at ∼406 nm was observed from 200 to 240 °C (trace 4 to 6) in Figure S10a1. According to the hard soft acid base (HSAB) principle, the dissociation energy of the bond of Zn−O (250 kJ/mol) is smaller than that of Mn−O (362 kJ/mol).[46] Hence, the carboxylate group (COO−) is easier to break up with Zn and then bind with Cd to form Cd(OA)$_1$(OAc)$_1$. The
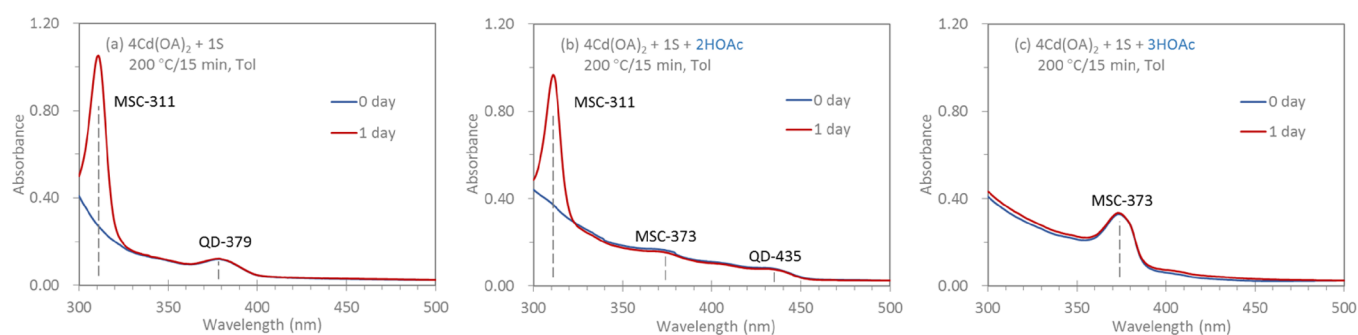
Figure 4. Optical absorption spectra of CdS samples (200 °C/15 min) extracted from three reaction batches with (a) no HOAc, (b) 2 equivalent of HOAc (0.30 mmol), and (c) 3 equivalent of HOAc (0.45 mmol) addition. The reaction contained $4Cd(OA)_2$ (0.60 mmol) and 1S (0.15 mmol), with a S concentration of 30 mmol/kg. The addition of HOAc was added at 120 °C, and sampling was performed after holding for 15 min at each temperature when the temperature was increased from 120 to 240 °C in steps of 20 °C. Absorption measurements (25 μL in 3.0 mL Tol) were performed immediately (blue traces, 0 day) and after 1 day storage (red traces, 1 day). It seems that the addition of HOAc promotes the formation of MSC-373 as well as suppresses the formation of MSC-311 and QDs.

results support the speculation that the ability to form $Cd(OA)_1(OAc)_1$ via ligand exchange influences the production of MSC-373. Figure S11 presents the batches with the usage of other Cd precursors of $Cd(SA)_2$ and $Cd(MA)_2$. The results reveal that the types of Cd sources before ligand exchange should have little effect on the products. In Figure S12, we explored the different feed molar ratios of Cd to S. It seems that the suitable ratios of Cd to S to produce MSC-373 were 2 and 4.

2.4. Effect of the Amount of HOAc Addition. To gain a deeper understanding of the formation of MSC-373, different amounts of HOAc addition were used. Figure 4 presents the absorption spectra of CdS samples (200 °C/15 min) from three reaction batches without (a) or with 0.30 (b) and 0.45 mmol (c) HOAc addition. The addition of HOAc was performed at 120 °C under a N_2 atmosphere. Afterward, the reaction temperature was increased from 120 to 240 °C in steps of 20 °C. Samples were taken at each temperature after 15 min had elapsed. Each sample (25 μL) was dispersed in Tol for absorption measurement immediately (blue traces) and after 1 day dispersion storage at room temperature (red traces). The spectra of all the samples are shown in Figure S13. In addition, Figure S14 presents the absorption spectra of CdS samples collected from the other three batches with the addition of 1.20 (a), 2.40 (b), and 3.60 mmol (c) HOAc.

In Figure 4a, without the HOAc addition, only CdS QDs, exhibiting a broad absorption peaking at 379 nm, were observed before storage (0 day, blue trace). After 1 day storage, MSC-311 evolved while QDs kept their absorption (1 day, red trace). In Figure 4b, with 0.30 mmol of HOAc, both QDs and a tiny amount of MSC-373 were observed before storage (0 day, blue trace). It was noteworthy that QDs exhibited a longer wavelength absorption peaking at 435 nm with a smaller density compared to that in Figure 4a. Similarly, after 1 day storage, MSC-311 evolved (1 day, red trace) with a smaller amount compared to that in Figure 4a. With 0.45 mmol of HOAc, MSC-373 was observed without the appearance of MSC-311 or QDs before storage (0 day, blue trace), as shown by Figure 4c. After 1 day storage, MSC-373 changed little and MSC-311 did not appear (1 day, red trace). The whole evolution of the three batches is presented in Figure S13. Without HOAc addition (Figure S13a), only QDs were observed when the temperature was increased from 200 to 240 °C (traces 5−7) before storage (0 day), with the redshift from 379 to 410 nm. After 1 day storage, MSC-311 appeared at 160

°C (trace 3) and increased to its largest density at 200 °C (trace 5) then decreased until 240 °C (trace 7). With 0.30 mmol HOAc addition (Figure S13b), both a tiny amount of MSC-373 and QDs were observed at relatively high temperatures (from 180 to 240 °C (traces 4−7)) before storage (0 day). MSC-373 developed at a fixed wavelength, while QDs grew with a redshift from 420 to 450 nm. After 1 day storage, MSC-311 appeared and developed in a similar pattern when the temperature was heated from 160 to 240 °C (traces 3−7). With 0.45 mmol HOAc addition (Figure S13c), only MSC-373 was observed from 160 to 240 °C (traces 3−7) before storage (0 day). After 1 day storage, MSC-311 was observed at 160 °C (trace 3). MSC-373 changed little from 160 to 240 °C (traces 3−7). In Figure S14, the density of MSC-373 appeared to increase with the amount of HOAc addition increasing.

The addition of HOAc plays a critical role in the formation of MSC-373 as well as suppressing the formation of MSC-311 and QDs. No signature of MSC-311 appeared in 0 day samples (blue traces) in Figure 4a,b. After 1 day incubation (red traces), MSC-311 was observed. According to the two-pathway model, MSCs are transformed from PCs, which are transparent in optical absorption. The PC-311 generated above 160 °C, during 1 day incubation, transformed to MSC-311 via intermolecular reorganization.[31] Furthermore, for the batches without (Figure S13a2) or with (Figure S13b2) 0.30 mmol of HOAc, the amount of MSC-311 decreased with the growth of QDs when the reaction temperature increased from 180 to 240 °C (traces 4−7). An individual formation pathway was proposed, which suggested that there existed an indirect conversion from MSC-311 into conventional QDs via PC-311. A tiny amount of MSC-373 was observed in Figure 4b. It seems that the addition of HOAc can facilitate the formation of MSC-373. Compared to Figure 4a, a relatively large size and small amount of QDs were observed, which was likely due to the formation of MSC-373. Usually, the formation of MSC-373 consumes PCs before the nucleation and growth of QDs, leading to a relatively low concentration of monomers.[23,42] According to the classical nucleation theory (CNT), the QDs are readily developed with a large size and small amount in a low concentration of monomer environment. Furthermore, the addition of a small amount HOAc (Figure 4c) hinders the formation of MSC-311 and the nucleation and growth of QDs. In a range of 0.30−4.80 mmol of HOAc, the larger the amount of HOAc added, the larger the amount of MSC-373 formed.
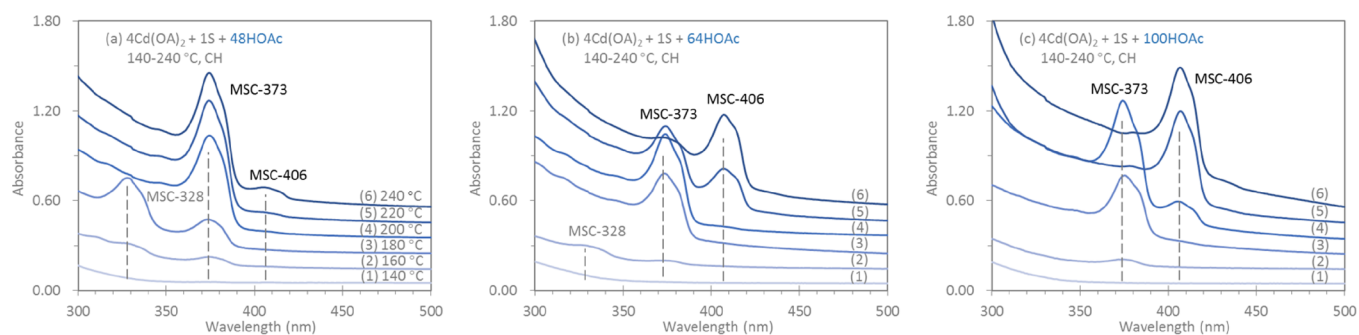
Figure 5. Evolution of optical absorption properties of CdS samples extracted from three batches with (a) 48 equivalent of HOAc (7.20 mmol), (b) 64 equivalent of HOAc (9.60 mmol), and (c) 100 equivalent of HOAc (15.00 mmol) addition. The reaction temperature was kept for 15 min after the addition performed at 120 °C, and sampling occurred at (1) 140 °C/15 min, (2) 160 °C/15 min, (3) 180 °C/15 min, (4) 200 °C/15 min, (5) 200 °C/15 min, and (6) 240 °C/15 min. For the spectroscopy study, an aliquot (25 μL) of each as-synthesized sample was dispersed in 3.0 mL of CH. Obviously, CdS MSC-406 was developed gradually when the HOAc addition was increased from 7.20 to 15.00 mmol.

Further increment of the HOAc amount results in the formation of another type of CdS MSCs. As shown in Figure 5, the samples were extracted from three reaction batches with 7.20 (a), 9.60 (b), and 15.00 (c) mmol of HOAc added; 25 μL of each sample was dispersed in CH for the spectroscopy study. In batch a, MSC-373 was observed initially at 160 °C (trace 2), together with the appearance of MSC-328. Afterward, MSC-373 kept developing till 220 °C (trace 5), while MSC-328 was completely gone at 200 °C (trace 4). At 240 °C (trace 6), the amount of MSC-373 decreased a little, accompanied by the appearance of MSC-406. In batch b, similarly, MSC-373 was initially observed at 160 °C (trace 2), coupled with the presence of MSC-328. MSC-373 continued forming when the temperature was elevated from 160 to 200 °C (traces 2−4), then started to decrease with the temperature increasing. MSC-406 started to appear at 220 °C (trace 5) and kept developing till 240 °C (trace 6). In batch c, MSC-373 kept increasing in amount when the temperature was increased from 160 to 200 °C (traces 2−4) and disappeared with the temperature increasing. MSC-406 started to form at 200 °C (trace 4) and continued to develop till 240 °C (trace 6). Figure S15 shows the absorption and emission spectra of MSC-406. The PL spectra of MSC-406 display a sharp band gap emission peak at 416 nm with trap emission at 541 nm. It seems that the larger amount of HOAc (from 7.20 to 15.00 mmol) addition favors the formation of MSC-406 instead.

3. CONCLUSIONS

In conclusion, the present study addresses the synthesis of colloidal photoluminescent CdS MSCs with carboxylic small molecule additives. With the addition of HOAc, CdS MSC-373, which exhibits optical absorption peaking at 373 nm and emission peaking at ∼385 nm, evolved without the coproduction of QDs. The as-synthesized MSC-373 was dot-like with the size of ∼2 nm in TEM images, which appeared as nanoflakes after purification with EtOH. We explored the effect of the carboxylic small molecules on the formation of MSC-373 and found that the acids with shorter carbon length favored the formation of MSC-373 and the use of $Zn(OAc)_2$ was more efficient than $Mn(OAc)_2$. Thus, we speculate that the ligand exchange on Cd from HOA to HOAc is the key factor for the evolution of MSC-373. The addition of HOAc facilitates the formation of MSC-373 and hinders the formation of MSC-311 and the nucleation and growth of QDs. Specifically, when the amount of HOAc was increased

from 0.30 to 4.80 mmol, the amount of MSC-373 increased. A further increase in HOAc amount from 7.20 to 15.00 mmol leads to the formation of MSC-406, another CdS MSCs with photoluminescence. In our previous study of CdTe MSC-427,[36] the effect of HOAc was proposed to control the synthesis selectivity of MSCs and QDs via ligand exchange, while in the present study, we found that the formation of CdS QDs might involve the PCs of MSC-311 PC of MSC-311. With the addition of HOAc, MSC-373 formed, which should be more stable, and will not transform to QDs. We believe that the present study will open up a new avenue to prepare a series of MSCs with photoluminescent property for various applications.[36,37,47,48] Also, the current study may inspire efforts to narrow the knowledge gap regarding the structure−property relationship of CdS MSCs and their possible transformations.[30,33,34,49,50]

4. METHODS

4.1. Chemicals. Cadmium oxide (CdO, 99.5%), oleic acid (HOA, 90.0%), hexanoic acid (C6 acid, 99.5%), myristic acid (MA, 99.0%), zinc acetate ($Zn(OAc)_2$, 99.99%), manganese acetate tetrahydrate ($Mn(OAc)_2·4H_2O$, 99.0%,), and 1-octadecene (ODE, $C_{18}H_{36}$, 90.0%) were purchased from Sigma-Aldrich. Sulfur powder (S, 99.5%), acetic acid (HOAc, CH_3COOH, 99.5%), stearic acid stearic acid (SA, 99.0%), ethanol (EtOH, 95%), and toluene (Tol, 99.5%) were purchased from Chengdu Kelong Chemical. Butyric acid (C4 acid, 99.0%) was purchased from Alfa Aesar, and cyclohexane (CH, 99.5%) was purchased from Tianjin Zhiyuan Chemical. All the chemicals were used as received without further purifications.

4.2. Cadmium Stock Solution. CdO (0.7704 g, 6.0 mmol), HOA (3.7285 g, 13.2 mmol), and ODE (5.0000 g) were loaded into a 50 mL three-neck flask. The mixture was degassed and backfilled with N_2 (99.0%), with such a procedure repeated three times at room temperature until no bubble was observed. Then, the reaction temperature was increased to 240 °C under a N_2 atmosphere to obtain a clear colorless solution. The resulting solution was cooled to 120 °C, held 30 min under vacuum, and then cooled to room temperature under N_2 for storage.

4.3. Synthesis of Photoluminescent CdS MSC-373. A mixture of $Cd(OA)_2$ (0.9512 g, 0.60 mmol), S powder (0.0048 g, 0.15 mmol), and ODE (3.7560 g) was placed in a 50 mL three-neck flask with a condenser. As is known, the boiling

point of HOAc is about 118 °C, and the use of a condenser helps HOAc to be evaporated back to the flask. The mixture was degassed and evacuated at room temperature for 30 min until no bubbles were observed. Under vacuum, the temperature was heated steadily to 120 °C and the mixture remained at this temperature for 30 min. Under a N_2 atmosphere, HOAc (0.2880 g, 4.80 mmol) was added into the flask, to achieve the feed molar ratio of 4Cd to 1S to 32acid, with a S concentration of 30 mmol/kg and total solution weight of 5.0 g. The reaction temperature was increased to 240 °C in steps of 20 °C. Samples were extracted after 15 min elapsed at each temperature. The reaction solution was transparent with a slightly ivory color after HOAc was added; the color turned red-brown with the temperature increasing.

4.4. Purification of CdS MSC-373. One as-synthesized sample (200 μL) was dispersed into 1.0 mL of Tol; then, 2.0 mL of EtOH was dropwise added. After centrifuging (9000 rpm for 3 min), the precipitate was collected. After the purification was repeated twice, the precipitate was dispersed in 2.0 mL of CH, and then 250 μL of which was extracted and dispersed in 3.0 mL of CH for characterization. Centrifugations were carried out on a Shuke Centrifuge TG-16S.

4.5. Characterization. For ultraviolet−visible (UV−vis) absorption, photoluminescence emission (PL), and photoluminescence excitation (PLE) measurement, typically, 25 μL of the as-synthesized sample was dispersed in 3.0 mL of CH/Tol. UV−vis absorption spectra were collected between 290 and 500 nm with intervals of 1 nm on a Hitachi UH4150 spectrometer, a Hitachi U-2910 spectrometer, or a UV 2310 II spectrometer. The PL and PLE spectra were recorded with a 1 nm interval on an ANGDONG F380 spectrometer (slit widths for excitation and emission are 5.0 nm) and Horiba Fluoromax-4 spectrometer (slit widths for excitation and emission are 2.5 nm). The quartz cuvettes (3.5 mL standard QS cells with the light path of 10 mm) were purchased from Hellma Analytics.

For transmission electron microscopy (TEM) measurement, 25 μL of the sample extracted at 200 °C /15 min was dispersed in 3.0 mL of CH. Then, one drop of the dispersion was placed on a TEM grid, which was then placed in a fume hood for about 10 min for the solvent evaporation. The TEM images were taken on a FEI Tecnai G2 F20 S-TWIN.

For Fourier transform infrared absorption spectroscopy (FTIR), samples were measured on a NEXUS 670 with a resolution of 4 cm^{-1}. A background scan was taken before each measurement (16 scans).

For energy-dispersive spectrometry (EDS) measurement, data were obtained using a Hitachi TM3000 microscope at 15 kV in Map mode.

For X-ray photoelectron spectroscopy (XPS) measurement, data were collected using an accelerating voltage of 15 kV and a current of 5 mA on AXIS Supra, Kratos. Al X-ray was its monochromatic source.

For powder X-ray diffraction (XRD) measurement, data were obtained using a Shimazu XRD-6100 diffractometer with Cu Kα radiation (λ = 1.5406 Å) at a rate of 10°/min between 10 and 90° in 2θ mode.

■ ASSOCIATED CONTENT

ⓢ Supporting Information

The Supporting Information is available free of charge at https://pubs.acs.org/doi/10.1021/acsomega.1c01362.

Experimental details of synthesis and characterization, including optical absorption, emission, TEM, FTIR, EDS, XPS, and XRD (PDF)

■ AUTHOR INFORMATION

Corresponding Authors

Chaoran Luan − *Laboratory of Ethnopharmacology, West China School of Medicine, Sichuan University, Chengdu, Sichuan 610065, P. R. China*; Email: luanchaoran@qq.com

Kui Yu − *Engineering Research Center in Biomaterials and Institute of Atomic and Molecular Physics, Sichuan University, Chengdu, Sichuan 610065, P. R. China; State Key Laboratory of Polymer Materials Engineering, Chengdu, Sichuan 610065, P. R. China*; ⓞ orcid.org/0000-0003-0349-2680; Email: kuiyu@scu.edu.cn

Authors

Zhengtian He − *Engineering Research Center in Biomaterials, Sichuan University, Chengdu, Sichuan 610065, P. R. China*

Dongqing Wang − *Engineering Research Center in Biomaterials, Sichuan University, Chengdu, Sichuan 610065, P. R. China*

Qiyu Yu − *College of Materials Science and Engineering, Sichuan University of Science and Engineering, Zigong, Sichuan 643000, P. R. China; State Key Laboratory of Polymer Materials Engineering, Chengdu, Sichuan 610065, P. R. China*; ⓞ orcid.org/0000-0001-9570-1755

Meng Zhang − *Institute of Atomic and Molecular Physics, Sichuan University, Chengdu, Sichuan 610065, P. R. China*; ⓞ orcid.org/0000-0002-2852-2527

Shanling Wang − *Analytical & Testing Center, Sichuan University, Chengdu, Sichuan 610065, P. R. China*

Wen Huang − *Laboratory of Ethnopharmacology, West China School of Medicine, Sichuan University, Chengdu, Sichuan 610065, P. R. China*; ⓞ orcid.org/0000-0002-9772-9492

Complete contact information is available at: https://pubs.acs.org/10.1021/acsomega.1c01362

Author Contributions

The manuscript was written through the contributions of all authors. All authors have given approval to the final version of the manuscript.

Notes

The authors declare no competing financial interest.

■ REFERENCES

(1) Brus, L. E. Electron-Electron and Electron-Hole Interactions in Small Semiconductor Crystallites: The Size Dependence of the Lowest Excited Electronic State. *J. Chem. Phys.* **1984**, *80*, 4403−4409.

(2) Doñate-Buendia, C.; Torres-Mendieta, R.; Pyatenko, A.; Falomir, E.; Fernández-Alonso, M.; Mínguez-Vega, G. Fabrication by Laser Irradiation in a Continuous Flow Jet of Carbon Quantum Dots for Fluorescence Imaging. *ACS Omega* **2018**, *3*, 2735−2742.

(3) Liu, W.; Howarth, M.; Greytak, A. B.; Zheng, Y.; Nocera, D. G.; Ting, A. Y.; Bawendi, M. G. Compact Biocompatible Quantum Dots Functionalized for Cellular Imaging. *J. Am. Chem. Soc.* **2008**, *130*, 1274−1284.

(4) Ouyang, J.; Kuijper, J.; Brot, S.; Kingston, D.; Wu, X.; Leek, D. M.; Hu, M. Z.; Ripmeester, J. A.; Yu, K. Photoluminescent Colloidal CdS Nanocrystals with High Quality via Noninjection One-Pot Synthesis in 1-Octadecene. *J. Phys. Chem. C* **2009**, *113*, 7579−7593.

(5) Ouyang, J.; Ratcliffe, C. I.; Kingston, D.; Wilkinson, B.; Kuijper, J.; Wu, X.; Ripmeester, J. A.; Yu, K. Gradiently Alloyed Zn$_x$Cd$_{1-x}$S Colloidal Photoluminescent Quantum Dots Synthesized via a Noninjection One-Pot Approach. *J. Phys. Chem. C* **2008**, *112*, 4908−4919.

(6) Ouyang, J.; Ripmeester, J. A.; Wu, X.; Kingston, D.; Yu, K.; Joly, A. G.; Chen, W. Upconversion Luminescence of Colloidal CdS and ZnCdS Semiconductor Quantum Dots. *J. Phys. Chem. C* **2007**, *111*, 16261−16266.

(7) Pandiyan, S.; Arumugam, L.; Srirengan, S. P.; Pitchan, R.; Sevugan, P.; Kannan, K.; Pitchan, G.; Hegde, T. A.; Gandhirajan, V. Biocompatible Carbon Quantum Dots Derived from Sugarcane Industrial Wastes for Effective Nonlinear Optical Behavior and Antimicrobial Activity Applications. *ACS Omega* **2020**, *5*, 30363−30372.

(8) Zhang, F.; Zhong, H.; Chen, C.; Wu, X.-G.; Hu, X.; Huang, H.; Han, J.; Zou, B.; Dong, Y. Brightly Luminescent and Color-Tunable Colloidal CH$_3$NH$_3$PbX$_3$ (X = Br, I, Cl) Quantum Dots: Potential Alternatives for Display Technology. *ACS Nano* **2015**, *9*, 4533−4542.

(9) Ouyang, J.; Zaman, M. B.; Yan, F. J.; Johnston, D.; Li, G.; Wu, X.; Leek, D.; Ratcliffe, C. I.; Ripmeester, J. A.; Yu, K. Multiple Families of Magic-Sized CdSe Nanocrystals with Strong Bandgap Photoluminescence via Noninjection One-Pot Syntheses. *J. Phys. Chem. C* **2008**, *112*, 13805−13811.

(10) Brus, L. Electronic Wave Functions in Semiconductor Clusters: Experiment and Theory. *J. Phys. Chem.* **1986**, *90*, 2555−2560.

(11) Kurihara, T.; Noda, Y.; Takegoshi, K. Capping Structure of Ligand-Cysteine on CdSe Magic-Sized Clusters. *ACS Omega* **2019**, *4*, 3476−3483.

(12) Liu, Y.; Rowell, N.; Willis, M.; Zhang, M.; Wang, S.; Fan, H.; Huang, W.; Chen, X.; Yu, K. Photoluminescent Colloidal Nanohelices Self-Assembled from CdSe Magic-Size Clusters via Nanoplatelets. *J. Phys. Chem. Lett.* **2019**, *10*, 2794−2801.

(13) Wang, R.; Calvignanello, O.; Ratcliffe, C. I.; Wu, X.; Leek, D. M.; Zaman, M. B.; Kingston, D.; Ripmeester, J. A.; Yu, K. Homogeneously-Alloyed CdTeSe Single-Sized Nanocrystals with Bandgap Photoluminescence. *J. Phys. Chem. C* **2009**, *113*, 3402−3408.

(14) Wang, R.; Ouyang, J.; Nikolaus, S.; Brestaz, L.; Zaman, M. B.; Wu, X.; Leek, D.; Ratcliffe, C. I.; Yu, K. Single-Sized Colloidal CdTe Nanocrystals with Strong Bandgap Photoluminescence. *Chem. Commun.* **2009**, 962−964.

(15) Yu, K. CdSe Magic-Sized Nuclei, Magic-Sized Nanoclusters and Regular Nanocrystals: Monomer Effects on Nucleation and Growth. *Adv. Mater.* **2012**, *24*, 1123−1132.

(16) Yu, Q.; Liu, C.-Y. Study of Magic-Size Cluster Mediated Formation of CdS Nanocrystals: Properties of the Magic-Size Clusters and Mechanism Implication. *J. Phys. Chem. C* **2009**, *113*, 12766−12771.

(17) Li, M.; Ouyang, J.; Ratcliffe, C. I.; Pietri, L.; Wu, X.; Leek, D. M.; Moudrakovski, I.; Lin, Q.; Yang, B.; Yu, K. CdS Magic-Sized Nanocrystals Exhibiting Bright Band Gap Photoemission via Thermodynamically Driven Formation. *ACS Nano* **2009**, *3*, 3832−3838.

(18) Cui, J.; Beyler, A. P.; Marshall, L. F.; Chen, O.; Harris, D. K.; Wanger, D. D.; Brokmann, X.; Bawendi, M. G. Direct Probe of Spectral Inhomogeneity Reveals Synthetic Tunability of Single-Nanocrystal Spectral Linewidths. *Nat. Chem.* **2013**, *5*, 602−606.

(19) Empedocles, S. A.; Neuhauser, R.; Shimizu, K.; Bawendi, M. G. Photoluminescence from Single Semiconductor Nanostructures. *Adv. Mater.* **1999**, *11*, 1243−1256.

(20) Kasuya, A.; Sivamohan, R.; Barnakov, Y. A.; Dmitruk, I. M.; Nirasawa, T.; Romanyuk, V. R.; Kumar, V.; Mamykin, S. V.; Tohji, K.; Jeyadevan, B.; Shinoda, K.; Kudo, T.; Terasaki, O.; Liu, Z.; Belosludov, R. V.; Sundararajan, V.; Kawazoe, Y. Ultra-Stable Nanoparticles of CdSe Revealed from Mass Spectrometry. *Nat. Mater.* **2004**, *3*, 99−102.

(21) Kudera, S.; Zanella, M.; Giannini, C.; Rizzo, A.; Li, Y.; Gigli, G.; Cingolani, R.; Ciccarella, G.; Spahl, W.; Parak, W. J.; Manna, L. Sequential Growth of Magic-Size CdSe Nanocrystals. *Adv. Mater.* **2007**, *19*, 548−552.

(22) Liu, M.; Wang, K.; Wang, L.; Han, S.; Fan, H.; Rowell, N.; Ripmeester, J. A.; Renoud, R.; Bian, F.; Zeng, J.; Yu, K. Probing Intermediates of the Induction Period Prior to Nucleation and Growth of Semiconductor Quantum Dots. *Nat. Commun.* **2017**, *8*, 15467.

(23) Wang, L.; Hui, J.; Tang, J.; Rowell, N.; Zhang, B.; Zhu, T.; Zhang, M.; Hao, X.; Fan, H.; Zeng, J.; Han, S.; Yu, K. Precursor Self-Assembly Identified as a General Pathway for Colloidal Semiconductor Magic-Size Clusters. *Adv. Sci.* **2018**, *5*, 1800632.

(24) Zhang, J.; Hao, X.; Rowell, N.; Kreouzis, T.; Han, S.; Fan, H.; Zhang, C.; Hu, C.; Zhang, M.; Yu, K. Individual Pathways in the Formation of Magic-Size Clusters and Conventional Quantum Dots. *J. Phys. Chem. Lett.* **2018**, *9*, 3660−3666.

(25) García-Rodríguez, R.; Hendricks, M. P.; Cossairt, B. M.; Liu, H.; Owen, J. S. Conversion Reactions of Cadmium Chalcogenide Nanocrystal Precursors. *Chem. Mater.* **2013**, *25*, 1233−1249.

(26) Lamer, V. K.; Dinegar, R. H. Theory, Production and Mechanism of Formation of Monodispersed Hydrosols. *J. Am. Chem. Soc.* **1950**, *72*, 4847−4854.

(27) Sanz, E.; Vega, C.; Espinosa, J. R.; Caballero-Bernal, R.; Abascal, J. L. F.; Valeriani, C. Homogeneous Ice Nucleation at Moderate Supercooling from Molecular Simulation. *J. Am. Chem. Soc.* **2013**, *135*, 15008−15017.

(28) Thanh, N. T. K.; Maclean, N.; Mahiddine, S. Mechanisms of Nucleation and Growth of Nanoparticles in Solution. *Chem. Rev.* **2014**, *114*, 7610−7630.

(29) Luan, C.; Gökçinar, Ö. Ö.; Rowell, N.; Kreouzis, T.; Han, S.; Zhang, M.; Fan, H.; Yu, K. Evolution of Two Types of CdTe Magic-Size Clusters from a Single Induction Period Sample. *J. Phys. Chem. Lett.* **2018**, *9*, 5288−5295.

(30) Zhang, B.; Zhu, T.; Ou, M.; Rowell, N.; Fan, H.; Han, J.; Tan, L.; Dove, M. T.; Ren, Y.; Zuo, X.; Han, S.; Zeng, J.; Yu, K. Thermally-Induced Reversible Structural Isomerization in Colloidal Semiconductor CdS Magic-Size Clusters. *Nat. Commun.* **2018**, *9*, 2499.

(31) Zhu, T.; Zhang, B.; Zhang, J.; Lu, J.; Fan, H.; Rowell, N.; Ripmeester, J. A.; Han, S.; Yu, K. Two-Step Nucleation of CdS Magic-Size Nanocluster MSC−311. *Chem. Mater.* **2017**, *29*, 5727−5735.

(32) Liu, S.; Yu, Q.; Zhang, C.; Zhang, M.; Rowell, N.; Fan, H.; Huang, W.; Yu, K.; Liang, B. Transformation of ZnS Precursor Compounds to Magic-Size Clusters Exhibiting Optical Absorption Peaking at 269 nm. *J. Phys. Chem. Lett.* **2020**, *11*, 75−82.

(33) Luan, C.; Tang, J.; Rowell, N.; Zhang, M.; Huang, W.; Fan, H.; Yu, K. Four Types of CdTe Magic-Size Clusters from One Prenucleation Stage Sample at Room Temperature. *J. Phys. Chem. Lett.* **2019**, *10*, 4345−4353.

(34) Zhang, H.; Luan, C.; Gao, D.; Zhang, M.; Rowell, N.; Willis, M.; Chen, M.; Zeng, J.; Fan, H.; Huang, W.; Chen, X.; Yu, K. Room-Temperature Formation Pathway for CdTeSe Alloy Magic-Size Clusters. *Angew. Chem., Int. Ed.* **2020**, *59*, 16943−16952.

(35) Zhu, D.; Hui, J.; Rowell, N.; Liu, Y.; Chen, Q. Y.; Steegemans, T.; Fan, H.; Zhang, M.; Yu, K. Interpreting the Ultraviolet Absorption

in the Spectrum of 415 nm-Bandgap CdSe Magic-Size Clusters. *J. Phys. Chem. Lett.* **2018**, *9*, 2818–2824.

(36) Chen, M.; Luan, C.; Zhang, M.; Rowell, N.; Willis, M.; Zhang, C.; Wang, S.; Zhu, X.; Fan, H.; Huang, W.; Yu, K.; Liang, B. Evolution of CdTe Magic-Size Clusters with Single Absorption Doublet Assisted by Adding Small Molecules during Prenucleation. *J. Phys. Chem. Lett.* **2020**, *11*, 2230–2240.

(37) Liu, Y.; Willis, M.; Rowell, N.; Luo, W.; Fan, H.; Han, S.; Yu, K. Effect of Small Molecule Additives in the Prenucleation Stage of Semiconductor CdSe Quantum Dots. *J. Phys. Chem. Lett.* **2018**, *9*, 6356–6363.

(38) Liu, Y.; Zhang, B.; Fan, H.; Rowell, N.; Willis, M.; Zheng, X.; Che, R.; Han, S.; Yu, K. Colloidal CdSe 0-Dimension Nanocrystals and Their Self-Assembled 2-Dimension Structures. *Chem. Mater.* **2018**, *30*, 1575–1584.

(39) Zhang, J.; Li, L.; Rowell, N.; Kreouzis, T.; Willis, M.; Fan, H.; Zhang, C.; Huang, W.; Zhang, M.; Yu, K. One-Step Approach to Single-Ensemble CdS Magic-Size Clusters with Enhanced Production Yields. *J. Phys. Chem. Lett.* **2019**, *10*, 2725–2732.

(40) Li, Z.; Qin, H.; Guzun, D.; Benamara, M.; Salamo, G.; Peng, X. Uniform Thickness and Colloidal-Stable CdS Quantum Disks with Tunable Thickness: Synthesis and Properties. *Nano Res.* **2012**, *5*, 337–351.

(41) Son, J. S.; Park, K.; Kwon, S. G.; Yang, J.; Choi, M. K.; Kim, J.; Yu, J. H.; Joo, J.; Hyeon, T. Dimension-Controlled Synthesis of CdS Nanocrystals: From 0D Quantum Dots to 2D Nanoplates. *Small* **2012**, *8*, 2394–2402.

(42) Gao, D.; Hao, X.; Rowell, N.; Kreouzis, T.; Lockwood, D. J.; Han, S.; Fan, H.; Zhang, H.; Zhang, C.; Jiang, Y.; Zeng, J.; Zhang, M.; Yu, K. Formation of Colloidal Alloy Semiconductor CdTeSe Magic-Size Clusters at Room Temperature. *Nat. Commun.* **2019**, *10*, 1674.

(43) Anderson, N. C.; Hendricks, M. P.; Choi, J. J.; Owen, J. S. Ligand Exchange and the Stoichiometry of Metal Chalcogenide Nanocrystals: Spectroscopic Observation of Facile Metal-Carboxylate Displacement and Binding. *J. Am. Chem. Soc.* **2013**, *135*, 18536–18548.

(44) Bhattacharyya, L.; Rohrer, J. S. *Applications of Ion Chromatography for Pharmaceutical and Biological Products*; John Wiley & Sons, Inc.: USA, 2012.

(45) Dean, J. A. *Lange's Handbook of Chemistry*; McGraw Hill Book Co.: New York, United States, 1985.

(46) Haynes, W. M. *CRC Handbook of Chemistry and Physics 97th Edition: A Ready-Reference Book of Chemical and Physical Data*; CRC Press: Boca Raton, 2017.

(47) Bruce, J. A.; Clapper, J. C. Conjugation of Carboxylated Graphene Quantum Dots with Cecropin P1 for Bacterial Biosensing Applications. *ACS Omega* **2020**, *5*, 26583–26591.

(48) Shen, G.; Du, Z.; Pan, Z.; Du, J.; Zhong, X. Solar Paint from TiO$_2$ Particles Supported Quantum Dots for Photoanodes in Quantum Dot-Sensitized Solar Cells. *ACS Omega* **2018**, *3*, 1102–1109.

(49) Jia, G.; Sitt, A.; Hitin, G. B.; Hadar, I.; Bekenstein, Y.; Amit, Y.; Popov, I.; Banin, U. Couples of Colloidal Semiconductor Nanorods Formed by Self-Limited Assembly. *Nat. Mater.* **2014**, *13*, 301–307.

(50) Wang, Y.; Zhou, Y.; Zhang, Y.; Buhro, W. E. Magic-Size II-VI Nanoclusters as Synthons for Flat Colloidal Nanocrystals. *Inorg. Chem.* **2015**, *54*, 1165–1177.